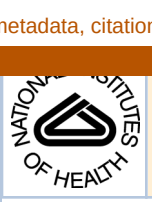

Published in final edited form as:

Neuroscience. 2010 September 1; 169(3): 987–993. doi:10.1016/j.neuroscience.2010.05.062.

A plasma membrane Ca^{2+} ATPase isoform at the postsynaptic density

Alain C. Burette[1], **Emanuel E. Strehler**[2], and **Richard J. Weinberg**[1,3]

[1]Department of Cell and Developmental Biology, University of North Carolina, Chapel Hill, NC 27599, USA

[2]Department of Biochemistry and Molecular Biology, Mayo Clinic College of Medicine, Rochester, MN 55905, USA

[3]Neuroscience Center, University of North Carolina, Chapel Hill, NC 27599, USA

Abstract

Most excitatory input in the hippocampus impinges on dendritic spines. Entry of Ca^{2+} into spines through NMDA receptors can trigger a sequence of biochemical reactions leading to sustained changes in synaptic efficacy. To provide specificity, dendritic spines restrict the diffusion of Ca^{2+} signaling and downstream molecules. The postsynaptic density (the most prominent subdomain within the spine) is the site of Ca^{2+} entry through NMDA receptors. We here demonstrate that Ca^{2+} can also be removed via pumps embedded in the postsynaptic density. Using light- and electron-microscopic immunohistochemistry, we find that PMCA2w, a member of the plasma membrane Ca^{2+}-ATPase family, concentrates at the PSD of most hippocampal spines. We propose that PMCA2w may be recruited into supramolecular complexes at the postsynaptic density, thus helping to regulate Ca^{2+} nanodomains at subsynaptic sites. Taken together, these results suggest a novel function for PMCAs as modulators of Ca^{2+} signaling at the synapse.

Keywords

calcium extrusion; calcium pump; immunohistochemistry; dendritic spine; postsynaptic density

Dendritic spines, the main target of excitatory synaptic input in the mammalian forebrain, compartmentalize a variety of calcium-regulated processes (Svoboda and Yasuda, 2006; Higley and Sabatini, 2008). Activation of glutamate receptors and voltage-dependent channels consequent to presynaptic glutamate release generates spine Ca^{2+} transients that control many aspects of postsynaptic signaling, including the induction of most forms of long-term potentiation and long-term depression (Cavazzini et al., 2005). Since the precise spatio-temporal structure of the Ca^{2+} signal is thought to determine the mode of plasticity (Malenka and Bear, 2004), it is critical to understand the mechanisms that shape $[Ca^{2+}]$ dynamics in synapses. However, in contrast to the extensive research addressing channels

Correspondence to: Alain Burette, Dept of Cell & Developmental Biology, University of North Carolina, CB # 7090, Chapel Hill, NC 27599; Phone: (919) 966 1277; Fax: (919) 966 1856; alain_burette@med.unc.edu.

that allow Ca^{2+} influx, our knowledge of the mechanisms that remove Ca^{2+} from synapses is very limited.

The plasma membrane Ca^{2+}-ATPase (PMCA) family of calcium pumps is the major high-affinity Ca^{2+} extrusion pathway in dendritic spines (Scheuss et al., 2006). PMCA-mediated Ca^{2+} extrusion in spines is activity-dependent, leading to [Ca^{2+}] dynamics that depend on the history of neuronal activity (Scheuss et al., 2006), potentially modulating the induction of synaptic plasticity. PMCA protein is expressed in dendritic spines (de Talamoni et al., 1993; Burette and Weinberg, 2007), but seems to concentrate away from the synapse; available anatomical evidence suggests that PMCAs are excluded from the postsynaptic density (PSD) (Burette and Weinberg, 2007), implying that Ca^{2+} entering at the synapse must undergo bulk diffusion through the spine cytoplasm before it can be extruded.

PMCAs belong to the IIB subfamily of P-type ATPases (Axelsen and Palmgren, 1998). In mammals, PMCA isoforms 1-4 are encoded by four separate genes; in all, more than 20 distinct PMCAs are generated through alternative splicing at two sites (A and C) (Strehler and Zacharias, 2001; Di Leva et al., 2008). Splicing at site A, which affects the first intracellular loop of the PMCA, is especially complex in PMCA2 (see Figure 1A). Inclusion of three optional exons leads to splice variant 2w. This splice, which occurs only in PMCA2, leads to a protein with 45 “extra” amino acid residues in the first intracellular loop. The functional significance of this extended loop is unclear, though recent evidence that the large w-insert directs PMCA2 to the apical membrane in kidney epithelial cells and cochlear hair cells suggests that this domain contributes to pump targeting (Chicka and Strehler, 2003; Grati et al., 2006; Hill et al., 2006).

Here we use light and electron microscopic immunohistochemistry to investigate the spatial distribution of the “w” variant of PMCA2 in the rat hippocampus. We find that PMCA2w concentrates at the PSD of excitatory synapses, where it may help sculpt Ca^{+2} nanodomains within spines.

EXPERIMENTAL PROCEDURES

Antibodies

Primary antibodies used included the rabbit polyclonal antibodies NR2 and anti-PMCA2w, which recognize PMCA2 (all splice variants) and 2w, respectively, and the guinea pig polyclonal anti VGLUT1 (Catalog No. AB5905, lot# 0507005922, Millipore, MA) and rabbit polyclonal anti-GABA (Catalog No. A2052, lot# 052K4827, Sigma, St. Louis, MO).

NR2 was generated against a 15-residue peptide sequence (TNSDFYSKNQRNESS, residues 5-19) in the amino terminus region of the rat PMCA2 (Filoteo et al., 1997). Its specificity was established by western blots using microsomes from COS cells overexpressing specific PMCAs, and further confirmed in microsomes from rat brain. NR2 recognizes two bands at 127 kDa and 132 kDa, corresponding to PMCA2a and PMCA2b, respectively.

The rabbit anti-PMCA2w antibody was raised against human PMCA2 peptides with C-terminal cysteine residues (PMCA2w: GDGLQLPAADGAAASNAADSC) (Hill, Williams et al. 2006). Peptides were synthesized in the Mayo Clinic Protein Core facility (Rochester, MN) and used to immunize two rabbits each (Cocalico Biologicals, Reamstown, PA). The antibody was affinity purified using positive and negative selection against peptides corresponding to rat PMCA2w (GDGLQLPAADGAAPANAAGSC) using methods described previously (Dumont, Lins et al. 2001). To verify NR2 and anti-PMCA2w specificity, we performed immunocytochemistry on brain sections from deafwaddler-2J

allele mutant mice (CByJ.A-Ttc7+? Atp2b2dfw-2J/J, stock # 002894, The Jackson Laboratory, Bar Harbor, ME), reported to lack PMCA2 mRNA and protein (Street et al., 1998), run in parallel with material from control mice and rats. Staining in the dfw2J mutant mice was extremely weak, and exhibited a "background" pattern unrelated to that seen for controls (data not shown).

The guinea pig anti-VGLUT1 antibody, raised against a C-terminus peptide of rat VGLUT1 (GATHSTVQPPRPPPPVRDY, (Melone et al. 2005)), recognizes a single band of Mr ~ 60,000 on immunoblots of synaptic membrane fractions from rat cerebral cortex. Double labeling experiments using this antibody and the well-characterized VGLUT1 antibody from RH Edwards (raised against a glutathione S-transferase fusion protein containing the last 68 amino acids of rat VGLT1, (Bellocchio et al. 1998)) show virtually complete colocalization (Melone et al., 2005). Furthermore, immunogold labeling shows that VGLUT1 immunoreactivity is selectively associated with axon terminals forming asymmetric synapses in cerebral cortex and hippocampus.

The anti-GABA antibody was raised in rabbit using GABA-BSA as the immunogen. The antibody was affinity-purified using the immunogen. It shows positive binding with GABA, and GABA-KLH in a dot blot assay, and negative binding with BSA (manufacturer's technical information).

Immunoblotting

Proteins were separated by SDS-PAGE and transferred to blotting membranes essentially as described previously (Dumont et al., 2001).

Tissue Preparation

All procedures related to the care and treatment of animals were in accordance with NIH guidelines, and were approved by the Institutional Animal Care and Use Committee. Male Sprague-Dawley rats (200-350 g, Charles River, Raleigh, NC) were deeply anesthetized with sodium pentobarbital (60 mg/kg, i.p.) and intracardially perfused with 4% paraformaldehyde in phosphate buffer (PB, 0.1 M, pH 7.4), for light microscopy (LM); with a mixture of 4% paraformaldehyde and 0.1% glutaraldehyde in PB, for double labeling with GABA; or with a mixture of 2% paraformaldehyde and 2% glutaraldehyde in PB, for EM. Brains were then removed and postfixed 2 h in the same fixative. Brains were cut at 40-60 μm on a Vibratome.

Light microscopy

Free-floating sections were permeabilized with 50% ethanol for 30 min and preincubated in 10% normal donkey serum (NDS, to block secondary antibody binding sites); sections were then incubated in primary antibody (PMCA2w, 1:2,000; PMCA2 1:1,000). Antigenic sites were visualized with a biotinylated secondary antibody (1:200; Jackson ImmunoResearch, West Grove, PA) followed by ExtrAvidin-peroxidase complex (1:5,000; Sigma); or by donkey IgG, conjugated to Cy-3 (1:200, Jackson ImmunoResearch; West Grove, PA). To study PMCA2w staining in relationship to dendritic spines, we used the membrane tracer DiO (Invitrogen), which labels even the finest neuronal processes. DiO crystals were applied with a micropipette directly to immunostained sections, which were then stored at 4°C for 24-72 h.

For double labeling with VGLUT, the second primary antibody (1:2,000, guinea pig anti-VGLUT1) was then applied overnight and visualized by a secondary antibody conjugated to Cy5 (1:200, Jackson ImmunoResearch). For double labeling with PMCA2w and GABA, tyramide signal amplification (TSA) was used (Burette et al., 2001). We used the PMCA2w

antibody at a concentration so low (1:50,000) that PMCA2w could not be detected by a conventional secondary antibody (donkey anti-rabbit IgG conjugated to FITC (1:200 for 3 hr, Jackson)), but was still clearly detectable with TSA. After overnight incubation in PMCA2w antibody, sections were processed (TSA direct kit, PerkinElmer LifeScience, Boston, MA), according to the manufacturer's recommendation. The second primary antibody (1:25,000; rabbit anti-GABA) was then applied overnight and visualized by donkey secondary antibody conjugated to Cy-3 (Jackson).

Sections were examined under a Leitz DMR microscope (Leica, Wetzlar, Germany) coupled to a 12-bit cooled charge-coupled device camera (Retiga EX, QImaging, Canada) and with a Leica SP2 confocal microscope. We used Corel Draw v.12 (Corel, Ontario, Canada) to sharpen images, adjust brightness and contrast, and compose final plates.

Electron microscopy

Fifty-micrometer-thick Vibratome sections were processed for osmium-free embedment. Sections were embedded in Epon-Spurr resin according to an osmium-free protocol described previously (Phend et al., 1992). Thin sections were cut and collected on 300-mesh uncoated nickel grids and stained for PMCA2w. After treatment with 4% paraphenylenediamine in Tris-buffered saline containing detergent (TBS/T; 0.02 M Tris, pH 7.6, 0.005%Tergitol NP-10) for 10 minutes, grids were rinsed and incubated overnight in primary antibody (1:2,000), rinsed in TBS/T, pH 7.6, transferred to TBS/T, pH 8.2, and incubated for 2 hr in goat anti-rabbit Fab fragments conjugated to 10 nm (GFAR10, BBInternational, United Kingdom) gold particles. Grids were then rinsed and counterstained with uranyl acetate and Sato's lead. In control experiments, in the absence of primary rabbit serum, virtually no gold particles were detected; after exposure to nonimmune rabbit serum, sparse gold particles were seen that showed no obvious pattern. Grids were examined on a Philips Tecnai 12 electron microscope at 80 kV accelerating voltage.

Image analysis

Analysis of punctate colocalization was performed according to Melone and co-workers (Melone et al., 2005). Briefly, immunofluorescence sections were examined with a Leica SP2 confocal microscope. Fields from CA1 hippocampus (stratum radiatum) were randomly selected, and Z-axis image stacks were acquired (z-step size 0.6 μm) as 1,024 × 1,024 pixel images, with a planapo ×63 objective (numerical aperture 1.4) and pinhole 1.0 Airy unit. To improve signal/noise ratio, 16 frames of each image were averaged. Microscopic fields were scanned with a pixel size of 60 nm. Quantitative analysis was performed in random 200 μm × 200 μm fields from each 1,024 × 1,024 pixel image. We performed all image processing in ImageJ (http://rsb.info.nih.gov/ij/, Rasband, 1997-2010).

Optimal visualization of punctate staining (good separation between contiguous puncta, along with clear contours for each immunopositive punctum) was achieved by setting the threshold for each color channel to the median pixel value over the field under study. This procedure was robust; with threshold values set anywhere between 0.5 and 2 times, the median pixel brightness had virtually no influence on the extent of colocalization or contact between puncta. Each confocal channel was examined individually, to identify immunopositive puncta. The two channels were then merged, and the presence or absence of colocalization or contacts was noted for each punctum. To further analyze PMCA2w distribution in 3D confocal stacks, we used ImageSurfer 1.13 (www.ImageSurfer.org); for details see Feng et al. (2007).

ImageJ was used for quantitative analysis of immunogold particles at synapses. To define "axodendritic" position, the distance between the center of each gold particle and the outer

leaflet of the postsynaptic membrane was measured. To define the "lateral" synaptic position of a gold particle, we measured the distance from each end of the PSD to a line drawn perpendicular to the synapse running through the center of the particle (Valtschanoff and Weinberg, 2001). Normalized lateral position of each gold particle within the axodendritic peak (from -30 nm to +60 nm from the postsynaptic membrane) L_N, was defined as $|(a-b)|/|(a+b)|$, where a and b are tangential distances along the plasma membrane from the center of the gold particle to the lateral edges of the synaptic specialization; thus L = 0 for gold particles at the center of the PSD, 1 for particles at its edge.

RESULTS

PMCA2w protein was detected throughout the rat forebrain and migrated as a single band of about 160 kDa in a Western blot of total rat forebrain extract (Fig. 1B). We focused our attention on the hippocampal CA1 subfield, whose pyramidal neurons exhibit several well-characterized forms of calcium-triggered synaptic plasticity. PMCA2w staining was uniformly distributed through CA1 (Fig. 1C), exhibiting a pattern that differed markedly from that of our previous work using a pan-PMCA2 antibody (Fig. 1D and Burette et al., 2003): PMCA2w staining was organized into numerous puncta throughout the neuropil (Fig. 1E), whereas overall staining for PMCA2 appeared as a fine layer outlining somata and dendrites (Fig 1F).

Double labeling experiments revealed a close relationship between these puncta and the presynaptic marker VGLUT1 (Fig. 2A, B), suggesting an association of PMCA2w with synapses. To assess the extent of this association, we analyzed 72 random fields (200 μm × 200 μm) in stratum radiatum of CA1. Of 1770 puncta immunopositive for PMCA2w, 1374 (78%) were likely to represent excitatory synapses, because they either overlapped or were adjacent to VGLUT-positive puncta. Approximatively 20% of PMCA2w puncta were not associated with VGLUT, raising the possibility that PMCA2w might also be present in inhibitory synapses. Analysis of 78 fields double-labeled for PMCA2w and GABA (Fig. 2C, D) confirmed this assumption: of 1480 puncta immunopositive for PMCA2w, 428 (29%) were likely to represent inhibitory synapses because they overlapped or were adjacent to GABA-positive puncta. Taken together, these data show that PMCA2w is strongly associated with synapses.

Since calcium transients in dendritic spines play a major role in synaptic processing, we investigated PMCA2w staining in relationship to spines. Double labeling with the membrane tracer DiO confirmed that dendritic spines in CA1 stratum radiatum contained PMCA2w (Fig. 3). Rather than being uniformly distributed within the spine, 3D analysis of confocal stacks showed that PMCA2w was typically at or near the plasma membrane, where it was restricted to a subregion of the spine head (Fig. 3B, C), as would be expected if it were associated with the PSD. Occasionally, local "hotspots" of PMCA2w could also be detected adjacent to the spine neck (arrowhead in Fig. $3B_5$), perhaps corresponding to GABAergic terminals.

To determine the location of PMCA2w more accurately, we performed electron microscopy, using post-embedding immunogold labeling. Labeling concentrated in dendritic spines, although immunoreactivity was also occasionally detected in presynaptic terminals. Only sparse labeling was found in dendrites and somata. In spines, PMCA2w concentrated over the PSD (Fig. 4A, B). Labeling was also detected within the cytoplasm of the spine head, associated with filaments of the actin network. Quantitative analysis of distribution revealed that PMCA2w immunogold particle density along the axo-dendritic axis was maximal over the PSD, with a peak about 20 nm inside the postsynaptic membrane, gradually diminishing into the postsynaptic cytoplasm. The lateral distribution of particle density was rather

uniform along the synapse, extending to ~0.3-0.4 normalized units (≤ 100 nm) beyond the edge of the PSD (Fig. 4D). There was no obvious relationship between lateral and tangential position of gold particles (Fig. 4E). Unexpectedly, we did not detect a significant correlation between synapse-associated antigen and length of synaptic profiles (Fig. 4F, $r^2 = 0.0074$), implying that small synapses contained a higher relative density of PMCA2w than did large synapses.

DISCUSSION

We investigated the distribution of PMCA2w in the rat hippocampus, finding that this pump concentrated in dendritic spines, where it associated with the postsynaptic density. To our knowledge this is the first direct evidence of a calcium pump embedded within the PSD.

Alternative splicing at the C-terminal splice site, which affects pump regulation, leads to two PMCA2 variants: PMCA2a and PMCA2b ((Strehler and Zacharias, 2001); see Fig. 1A). Since PMCA2a is restricted to GABAergic synapses (Burette et al., 2009), we infer that the observed PMCA2w staining within hippocampal spines represents the PMCA2w/b splice variant. In contrast to PMCA2a, PMCA2b has a PDZ (PSD-95/Dlg/ZO-1) domain binding motif at its C terminus that can interact with multiple scaffolding and signaling proteins (Strehler et al., 2007). Biochemical data show that PMCA2b binds with high affinity to PDZ domains of several members of the membrane-associated guanylate kinase protein family, including SAP90/PSD-95, SAP93/chapsyn-110, and SAP97/hDlg (DeMarco and Strehler, 2001). These scaffolds organize a variety of other signaling proteins in the PSD, including the NMDA receptor (NMDAR) (Kim and Sheng, 2004), thus allowing co-assembly of PMCA2 and NMDAR within the same membrane microdomain. In this context, it is striking that the relationship we observe between PSD length and PMCA2w density closely resembles that previously reported for PSD length and NMDAR density (Takumi et al., 1999; Kharazia and Weinberg, 1999). Taken together, these data suggest that PMCA2w/b within the synapse lies close to the NMDAR.

Ca^{2+} entry through NMDARs generates transient calcium nanodomains that selectively activate signaling complexes (Augustine et al., 2003; Keller et al., 2008); the temporo-spatial structure of these nanodomains may be a crucial determinant of the degree and nature of synaptic plasticity. By regulating extrusion of the Ca^{2+} entering the spine through NMDARs, we speculate that PMCA2w/b can modulate this Ca^{2+} nanodomain, though lack of satisfactory pharmacological agents makes it difficult to provide direct experimental evidence. However, an analogous function has been demonstrated in the heart, where a spatial linkage of PMCA4b to the calcium-dependent enzyme nNOS controls nNOS activity by regulating its Ca^{2+} microenvironment (Mohamed et al., 2009). The localization of PMCA2w/b at the PSD, where it may bind to numerous signaling molecules, suggests that it functions as local regulator of Ca^{2+} nanodomains at discrete subsynaptic sites, rather than as a global regulator of intracellular calcium.

Acknowledgments

Grant sponsor: NIH NS#39444 (RJW), NS51769 (EES). AB examined and analyzed the microscopic material, prepared plates, and wrote the manuscript. EES supplied PMCA2w antibody, prepared the western blots, and helped with manuscript writing. RJW helped with manuscript writing and data analysis. The authors thank S. Grand and K. Phend for histological support.

References

Augustine GJ, Santamaria F, Tanaka K. Local calcium signaling in neurons. Neuron 2003;40:331–346. [PubMed: 14556712]

Axelsen KB, Palmgren MG. Evolution of substrate specificities in the P-type ATPase superfamily. J Mol Evol 1998;46:84–101. [PubMed: 9419228]

Burette A, Weinberg RJ. Perisynaptic organization of plasma membrane calcium pumps in cerebellar cortex. J Comp Neurol 2007;500:1127–1135. [PubMed: 17183553]

Burette A, Khatri L, Wyszynski M, Sheng M, Ziff EB, Weinberg RJ. Differential cellular and subcellular localization of ampa receptor-binding protein and glutamate receptor-interacting protein. J Neurosci 2001;21:495–503. [PubMed: 11160429]

Burette AC, Strehler EE, Weinberg RJ. "Fast" plasma membrane calcium pump PMCA2a concentrates in GABAergic terminals in the adult rat brain. J Comp Neurol 2009;512:500–513. [PubMed: 19025983]

Cavazzini M, Bliss T, Emptage N. Ca^{2+} and synaptic plasticity. Cell Calcium 2005;38:355–367. [PubMed: 16154476]

Chicka MC, Strehler EE. Alternative splicing of the first intracellular loop of plasma membrane Ca^{2+}-ATPase isoform 2 alters its membrane targeting. J Biol Chem 2003;278:18464–18470. [PubMed: 12624087]

de Talamoni N, Smith CA, Wasserman RH, Beltramino C, Fullmer CS, Penniston JT. Immunocytochemical localization of the plasma membrane calcium pump, calbindin-D28k, and parvalbumin in Purkinje cells of avian and mammalian cerebellum. Proc Natl Acad Sci U S A 1993;90:11949–11953. [PubMed: 8265654]

DeMarco SJ, Strehler EE. Plasma membrane Ca^{2+}-atpase isoforms 2b and 4b interact promiscuously and selectively with members of the membrane-associated guanylate kinase family of PDZ (PSD95/Dlg/ZO-1) domain-containing proteins. J Biol Chem 2001;276:21594–21600. [PubMed: 11274188]

Di Leva F, Domi T, Fedrizzi L, Lim D, Carafoli E. The plasma membrane Ca^{2+} ATPase of animal cells: structure, function and regulation. Arch Biochem Biophys 2008;476:65–74. [PubMed: 18328800]

Dumont RA, Lins U, Filoteo AG, Penniston JT, Kachar B, Gillespie PG. Plasma membrane Ca^{2+}-ATPase isoform 2a is the PMCA of hair bundles. J Neurosci 2001;21:5066–5078. [PubMed: 11438582]

Feng D, Marshburn D, Jen D, Weinberg RJ, Taylor RM 2nd, Burette A. Stepping into the third dimension. J Neurosci 2007;27:12757–12760. [PubMed: 18032646]

Filoteo AG, Elwess NL, Enyedi A, Caride A, Aung HH, Penniston JT. Plasma membrane Ca^{2+} pump in rat brain. Patterns of alternative splices seen by isoform-specific antibodies. J Biol Chem 1997;272:23741–23747. [PubMed: 9295318]

Grati M, Aggarwal N, Strehler EE, Wenthold RJ. Molecular determinants for differential membrane trafficking of PMCA1 and PMCA2 in mammalian hair cells. J Cell Sci 2006;119:2995–3007. [PubMed: 16803870]

Higley MJ, Sabatini BL. Calcium signaling in dendrites and spines: practical and functional considerations. Neuron 2008;59:902–913. [PubMed: 18817730]

Hill JK, Williams DE, LeMasurier M, Dumont RA, Strehler EE, Gillespie PG. Splice-site A choice targets plasma-membrane Ca^{2+}-ATPase isoform 2 to hair bundles. J Neurosci 2006;26:6172–6180. [PubMed: 16763025]

Keller DX, Franks KM, Bartol TM Jr, Sejnowski TJ. Calmodulin activation by calcium transients in the postsynaptic density of dendritic spines. PLoS One 2008;3:e2045. [PubMed: 18446197]

Kharazia VN, Weinberg RJ. Immunogold localization of AMPA and NMDA receptors in somatic sensory cortex of albino rat. J Comp Neurol 1999;412:292–302. [PubMed: 10441757]

Kim E, Sheng M. PDZ domain proteins of synapses. Nat Rev Neurosci 2004;5:771–781. [PubMed: 15378037]

Malenka RC, Bear MF. LTP and LTD: an embarrassment of riches. Neuron 2004;44:5–21. [PubMed: 15450156]

Melone M, Burette A, Weinberg RJ. Light microscopic identification and immunocytochemical characterization of glutamatergic synapses in brain sections. J Comp Neurol 2005;492:495–509. [PubMed: 16228991]

Mohamed TM, Oceandy D, Prehar S, Alatwi N, Hegab Z, Baudoin FM, Pickard A, Zaki AO, Nadif R, Cartwright EJ, Neyses L. Specific role of neuronal nitric-oxide synthase when tethered to the

plasma membrane calcium pump in regulating the beta-adrenergic signal in the myocardium. J Biol Chem 2009;284:12091–12098. [PubMed: 19278978]

Phend KD, Rustioni A, Weinberg RJ. An osmium-free method of epon embedment that preserves both ultrastructure and antigenicity for post-embedding immunocytochemistry. J Histochem Cytochem 1995;43:283–292. [PubMed: 7532656]

Phend KD, Weinberg RJ, Rustioni A. Techniques to optimize post-embedding single and double staining for amino acid neurotransmitters. J Histochem Cytochem 1992;40:1011–1020. [PubMed: 1376741]

Rasband, WS.; Image, J. US National Institutes of Health. Bethesda, Maryland, USA: 1997-2008. http://rsb.info.nih.gov/ij/

Scheuss V, Yasuda R, Sobczyk A, Svoboda K. Nonlinear [Ca^{2+}] signaling in dendrites and spines caused by activity-dependent depression of Ca^{2+} extrusion. J Neurosci 2006;26:8183–8194. [PubMed: 16885232]

Strehler EE, Zacharias DA. Role of alternative splicing in generating isoform diversity among plasma membrane calcium pumps. Physiol Rev 2001;81:21–50. [PubMed: 11152753]

Strehler EE, Caride AJ, Filoteo AG, Xiong Y, Penniston JT, Enyedi A. Plasma membrane Ca^{2+} ATPases as dynamic regulators of cellular calcium handling. Ann NY Acad Sci 2007;1099:226–236. [PubMed: 17446463]

Svoboda K, Yasuda R. Principles of two-photon excitation microscopy and its applications to neuroscience. Neuron 2006;50:823–839. [PubMed: 16772166]

Takumi Y, Ramirez-Leon V, Laake P, Rinvik E, Ottersen OP. Different modes of expression of AMPA and NMDA receptors in hippocampal synapses. Nat Neurosci 1999;2:618–624. [PubMed: 10409387]

Valtschanoff JG, Weinberg RJ. Laminar organization of the NMDA receptor complex within the postsynaptic density. J Neurosci 2001;21:1211–1217. [PubMed: 11160391]

Xiong Y, Antalffy G, Enyedi A, Strehler EE. Apical localization of PMCA2w/b is lipid raft-dependent. Biochem Biophys Res Commun 2009;384:32–36. [PubMed: 19379709]

Abbreviations

GABA	γ-Aminobutyric acid
EM	electron microscopy
LM	light microscopy
NMDAR	N-methyl-D-aspartic acid receptor
NDS	normal donkey serum
nNOS	neuronal nitric oxide synthase
PDZ	PSD-95/Dlg/ZO-1
PB	phosphate buffer
PMCA	plasma membrane Ca^{2+}-ATPase
PSD	postsynaptic density
VGLUT	vesicular glutamate transporter

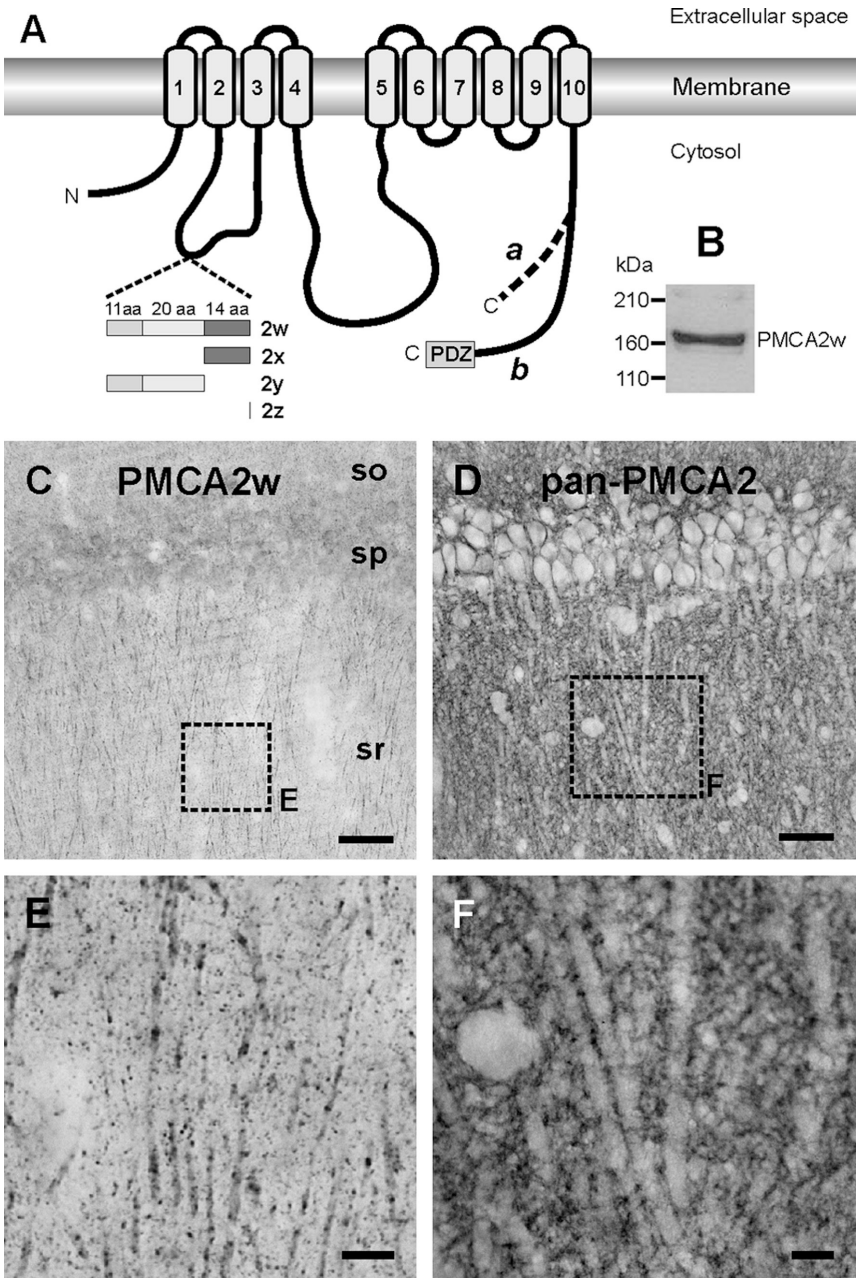

Figure 1.

A: Scheme of alternative splice variants of PMCA2. The ten transmembrane segments are indicated by gray cylinders, and the membrane bilayer is denoted by two horizontal bars. Alternative splicing of the first intracellular loop generates isoforms 2w, 2x, 2y, and 2z by insertion of 0-45 amino acids (aa) encoded by three separate exons (shown as boxes with numbers of encoded aa). Alternative splicing of the C-terminal tail results in variants “a” and “b” with different C-terminal sequences. The “b” splice variant contains a PDZ domain-binding motif (PDZ) at its C-terminus.

B: Western blot of 30 μg of total protein lysate from rat forebrain. The blot was probed with the rabbit polyclonal antibody specific for PMCA2w. The position of molecular weight standards is indicated on the left.

C-F: PMCA2w localizes in distinct puncta in the hippocampal CA1 region. Both PMCA2w (**C**) and total PMCA2 (**D**) are detected in all layers of CA1. However, PMCA2w immunostaining is organized into numerous puncta (**E**) while overall PMCA2 staining appeared as a thin layer outlining somata and dendrites (**F**).
SO, stratum oriens, SP; pyramidal cell layer; SR, stratum radiatum.
Scale bars, 50 μm in C and D; 5 μm in E; 10 μm in F.

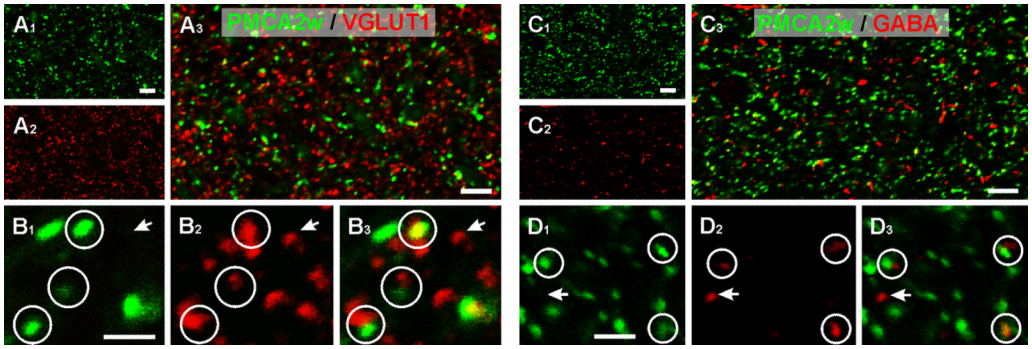

Figure 2.

PMCA2w labeling is associated with synapses. To define the nature of PMCA2w puncta, double labeling was performed for PMCA2w with VGLUT1 (**A**, **B**) and GABA (**C**, **D**). Double labeling shows that most PMCA2w puncta (green) are closely apposed to, or partially overlap with, the vesicular glutamate transporter (VGLUT, red), suggesting that PMCA2w concentrates at synaptic sites (**A**, circles in **B**). However, some VGLUT puncta were not associated with PMCA2w puncta (arrows in **B**).

Double labeling for PMCA2w and GABA (red, **C**) shows that most PMCA2w puncta are not associated with GABA puncta (**D**). In contrast, most GABA puncta (but not all, arrow) are closely apposed to, or overlap with, PMCA2w puncta (circles in **D**).

Scale bars: 10 μm in A and C; 2 μm in B and D.

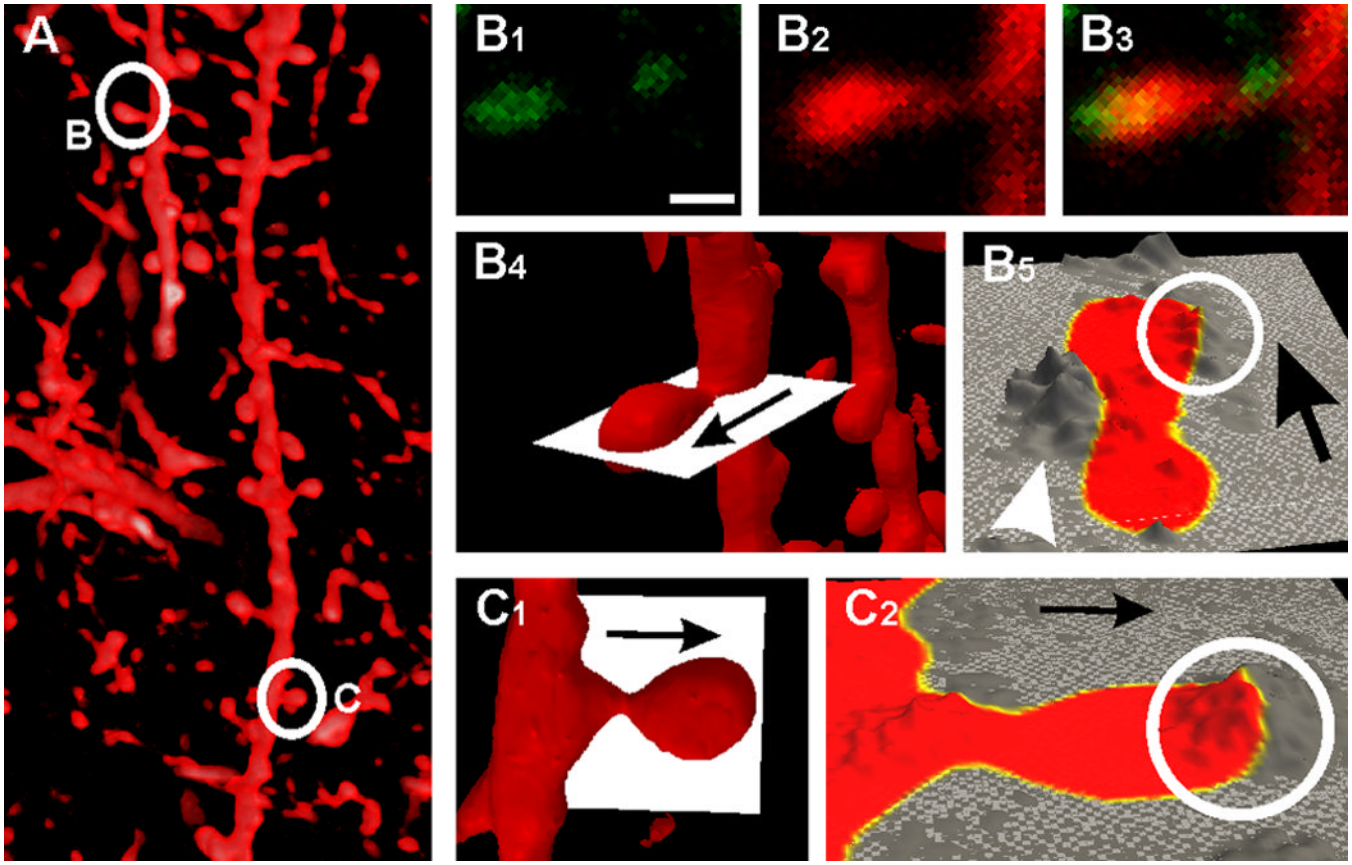

Figure 3.

PMCA2w puncta map to discrete regions on dendritic spines. The lipophilic tracer DiO (**A**, direct projection from a stack of 41 confocal images) was used to label the dendritic plasma membrane of CA1 pyramidal cells. Visual inspection of a single confocal image showing a PMCA2w punctum lying directly over a spine head (marked B in left panel) is shown in B_1-B_3. Note small PMCA punctum adjacent to the spine neck. 3D analysis of the full confocal stack confirms this pattern (**B_{4-5}**, **C_{1-2}**). The "slice extractor" (white plane) in **B_4** and **C_1** was interactively positioned through the two spines (marked B and C in left panel) B and C in **A**. The extracted slice is displayed as height field in **B_5** and **C_2**; the color map shows the outline of the spine as defined by DiO staining (yellow, the highest DiO intensity, marks the plasma membrane) and height displays the corresponding PMCA2w value (mountains represent high concentrations of PMCA2w, and valleys represent low concentrations). PMCA2w concentrates in a "hot spot" associated with the plasma membrane of the spine head (S, circle in **B_5**, **C_2**). Occasionally, PMCA2w concentrates outside the spine adjacent to the plasma membrane of the neck (arrowhead in **B_5**).

Scale bar: 0.5 μm in B.

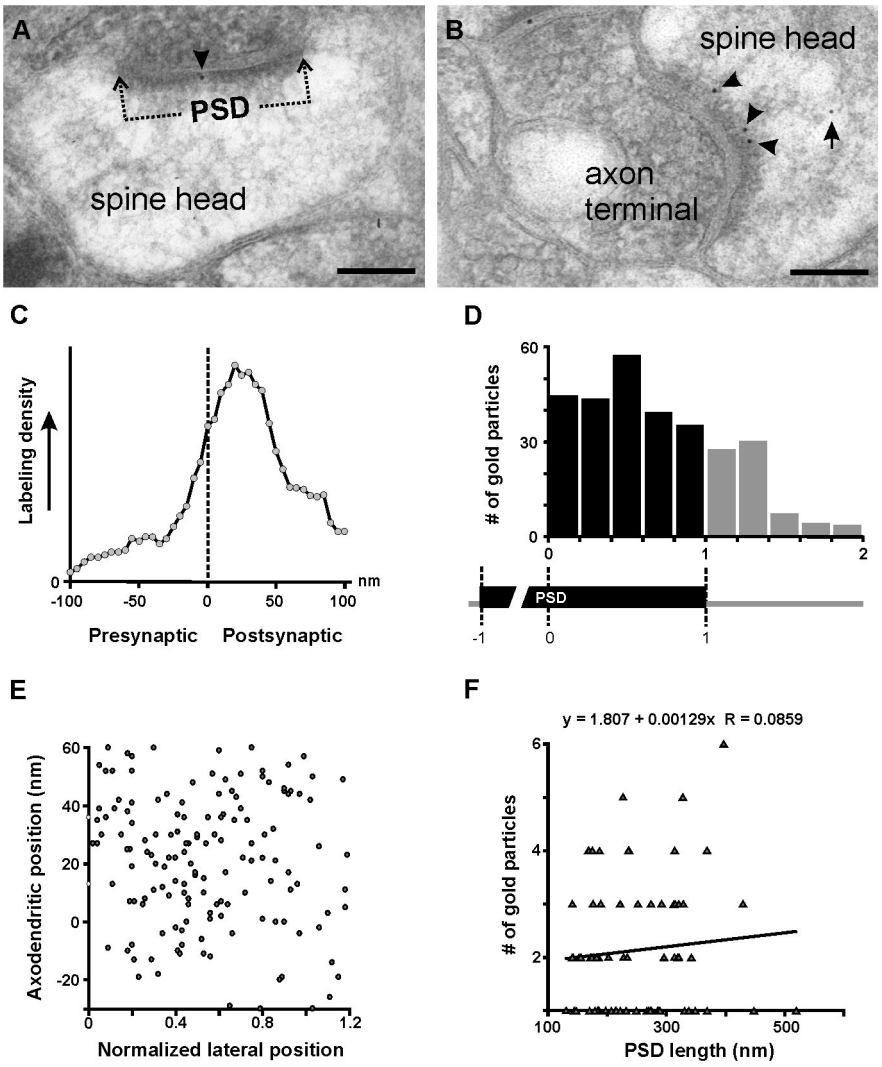

Figure 4.

Ultrastructural analysis using immunogold electron microscopy reveals association of PMCA2w with the postsynaptic density (PSD). Within spines, gold particles coding for PMCA2w are often at the membrane within the PSD (arrowheads in **A**, **B**). PMCA2w is also detected at extrasynaptic membrane and within the spine head (arrow in **B**). Quantitative analysis shows that immunogold labeling lies preferentially in the vicinity of the synaptic specialization, at highest concentration just inside the postsynaptic membrane (**C**). The lateral distribution of particle density (black bars) is rather uniform along the PSD (**D**), extending to ~0.3-0.4 normalized units beyond the edge of the PSD (gray bars in **D**). Scatterplot (**E**) shows no obvious relationship between lateral and axodendritic positions. Scatterplot (**F**) shows minimal relationship between length of synaptic profile and number of synapse-associated gold particles. Scale bars: 100 nm in A and B.